Journal of Colloid and Interface Science 629 (2023) 534–540

Contents lists available at ScienceDirect

Journal of Colloid and Interface Science

journal homepage: www.elsevier.com/locate/jcis

Carrier concentration-dependent interface engineering for high-performance zinc oxide piezoelectric device

Hongrui Zhang, Guo Tian, Da Xiong, Tao Yang, Shenglong Wang, Yue Sun, Long Jin, Boling Lan, Lin Deng, Weiqing Yang, Weili Deng *

Key Laboratory of Advanced Technologies of Materials (Ministry of Education), School of Materials Science and Engineering, Southwest Jiaotong University, Chengdu 610031, China

GRAPHICAL ABSTRACT

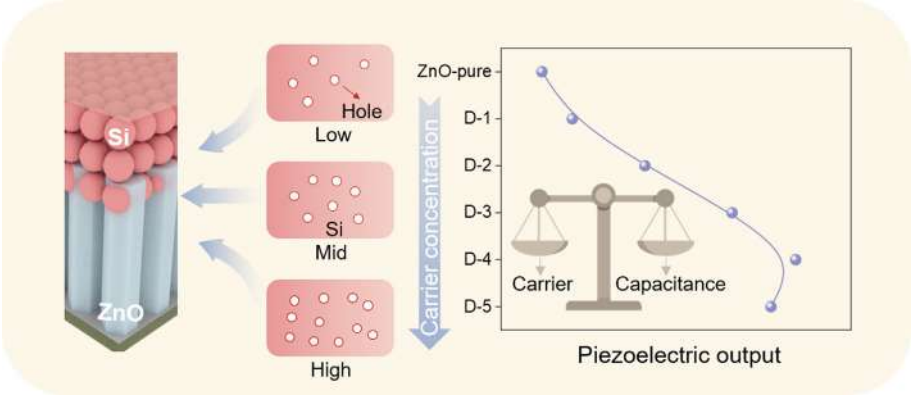

ARTICLE INFO

Article history:
Received 29 June 2022
Revised 6 August 2022
Accepted 30 August 2022
Available online 5 September 2022

Keywords:
Piezoelectric semiconductor
Carrier concentration
ZnO nanorods
Interface engineering
p-n junction

ABSTRACT

Piezoelectric semiconductor zinc oxide (ZnO) shows promising applications in many fields, however, its excellent piezoelectric performance is limited by the intrinsic screening effect. Forming p-n junction through interface engineering is an effective strategy to enhance its piezoelectric output, but the unclear regulation mechanism is a bottleneck in developing high-performance devices. In this work, the enhancement mechanism of interface engineering on the piezoelectric performance of ZnO nanorods (NRs) based devices is revealed from the perspective of carrier concentration. Both the theoretical and experimental results show that the piezoelectric output is significantly correlated with the carrier concentration, which is mainly attributed to the suppression of screening effect and the modulation of the device capacitance. After a reasonable matching design of carrier concentration, the piezoelectric potential of the ZnO NRs-based device is greatly enhanced by about 12 times. Apparently, these findings provide a fresh insight to further understand the enhancement mechanism of interface engineering on the electrical output of piezoelectric semiconductor devices, and provide effective support for the design of p-n junction piezoelectric devices.

1. Introduction

With the rapid development of flexible electronics, functional materials have been developed significantly in recent years [1–3].

* Corresponding author.
E-mail address: weili1812@swjtu.edu.cn (W. Deng).

https://doi.org/10.1016/j.jcis.2022.08.181
0021-9797/

Among them, piezoelectric materials are widely studied due to their excellent electromechanical coupling efficiency, fast response capability and self-powered characteristics [4–9]. Especially, piezoelectric semiconductor materials such as ZnO, GaN and CdS demonstrate greater advantages over insulating piezoelectric materials in many fields [10,11], such as piezoelectric transistors [12,13], piezotronics [14–17], piezo-phototronics [18–20], due to the attractive coupling of piezoelectric and semiconductor properties. However, the presence of intrinsic carriers in such materials induces a screening effect that weakens the piezoelectric output, which is one of the major challenges at hand. In the case of ZnO, the piezoelectric potential appears at both ends of the c-axis under external forces, but the directional migration of its intrinsic free carriers neutralizes the piezoelectric potential and therefore weakens the piezoelectric output [21,22]. To this end, a great deal of effort has been devoted to improving the output performance of ZnO-based piezoelectric devices [23,24]. Typically, the formation of p-n junction through interface engineering has proven to be an effective means of suppressing screening effect and improving the electrical output of ZnO-based piezoelectric devices [25–27]. A range of p-type semiconductor materials (such as CuI, NiO, PEDOT:PSS, P_3HT) have been used to improve the piezoelectric performance by forming p-n junctions on the surface of ZnO NRs [28–31]. Theoretically, the properties of p-n junctions are not only related to the material type, but also closely related to the carrier concentration of the material. However, there are few studies on the effect of carrier concentration of materials on the performance of piezoelectric devices, leading to the mechanism of interface engineering to regulate piezoelectric performance is still unclear. As a result, it is difficult to design high-performance device rationally.

In this work, we selected a series of p-type silicon (Si) as the counterpart to form p-n junctions with ZnO and focused on the effect of carrier concentration on the piezoelectric outputs. The enhancement mechanism of carrier concentration-dependent interface engineering on piezoelectric performance was theoretically and experimentally revealed in terms of depletion region, built-in electric field and junction capacitance. As a result, the piezoelectric potential of ZnO-Si p-n junction device was significantly improved by about 12 times with the matched carrier concentration. Here, we believe that these findings can provide reasonable ideas for the efficient design of p-n junction devices and are expected to promote further development of piezoelectric semiconductor devices in the future.

2. Experimental section

Synthesis of ZnO NRs and preparation of ZnO-Si p-n junction piezoelectric devices. ZnO NRs were synthesized using the low-temperature hydrothermal method as previously reported [32]. First, polyethylene naphthalate (PEN) substrate with indium tin oxide (ITO) as the bottom electrode was cleaned with deionized water and ethanol. Then, a ZnO seed layer was deposited on the ITO by radio frequency (RF) magnetron sputtering. Next, the PEN substrates sputtered with the ZnO seed layer were immersed in a nutrient solution at 85 °C for 6 h, where the nutrient solution consisted of 0.075 M zinc nitrate hexahydrate ($Zn(NO_3)_2$-$6H_2O$) (Sinopharm Chemical Reagent Co., Ltd, AR, ≥99.0%) and hexamethylenetetramine (Sinopharm Chemical Reagent Co., Ltd, AR, ≥99.0%). Subsequently, it was washed with deionized water and then dried in an oven at 50 °C. Then, five p-type Si films with different doping concentrations were deposited on the surface of the ZnO NRs by RF magnetron sputtering. During the deposition, the working pressure, RF power, and gas flow rate were kept at 1.5 Pa, 100 W, and 30 sccm, respectively. To prevent the device from short-circuiting, a thin layer of polymethyl methacrylate (PMMA) (Aladdin) was spin-coated on the surface of p-type Si films. Finally, the ZnO-Si p-n junction piezoelectric devices were encapsulated by polyurethane films after sputtering Ag as the top electrode.

Materials characterization. The morphology of the synthesized materials was characterized by scanning electron microscope (SEM, JEOL JSM7800F). The type and distribution of elements on the surface and cross-section of the samples were obtained by energy dispersive X-ray spectrometer (EDS, probe of Oxford Instrument). X-ray diffraction (XRD, DX-1000 diffractometer) and Raman spectra (HORIBA Jobin-Yvon XploRA ONE) were used to determine the phase structure of the samples. In addition, Mott-Schottky (M-S) plots and impedance spectra were obtained by the CHI660E electrochemical station. *I-V* curves were obtained by a Keithley 4200 semiconductor test system.

Device measurements. For electromechanical testing, a linear motor (HS01-37 × 166) applied pressure perpendicular to the sample and this pressure was measured by a digital dynamometer (Mark-10, MR03-10). The open circuit voltages and short circuit currents generated by the devices were collected by Keithley 6514 in real time. The relevant simulation in this work was implemented by the COMSOL software package.

3. Results and discussion

Fig. 1**a** depicts a schematic diagram of ZnO-based p-n junction piezoelectric device. The p-n junction is formed by sputtering a p-type semiconductor Si film on the surface of the ZnO NRs, taking advantage of the easy tuning of the Si film carrier concentration. Fig. 1**b** illustrates the detailed preparation of the p-n junction device, including magnetron deposition of ZnO seed layer on the PEN substrate with ITO bottom electrode, low-temperature hydrothermal growth of ZnO NRs, magnetron sputtering of p-type Si film and Ag top electrode. The distribution of carriers in the junction region of ZnO-Si device is schematically shown in Fig. 1**c**. At the interface of ZnO-Si, free electrons from the surface of ZnO NRs tend to diffuse into Si, and holes from the Si surface tend to diffuse into the ZnO NRs due to the difference of carrier concentration. When the electrons and holes at the interface reach dynamic equilibrium, a depletion region and a built-in electric field are formed, which directly affects the suppression of the screening effect. Obviously, both the depletion region and the built-in electric field are closely linked to the carrier concentration of the semiconductor material. Therefore, Si films with different carrier concentrations were chosen as p-type semiconductor materials to enhance piezoelectric output by forming p-n junctions (Fig. 1**d**). Five p-type Si films with different carrier concentrations were obtained by RF magnetron sputtering, defined as S-1, S-2, S-3, S-4, S-5, and the corresponding ZnO-Si p-n junction devices were defined as D-1, D-2, D-3, D-4, D-5, respectively. Fig. 1**e (i)** illustrates the presence of large number of free electrons in intrinsic ZnO NRs, which is the root cause of the screening effect. The formation of depletion region and the built-in electric field in ZnO-Si p-n junction devices will consume some of the free electrons in ZnO NRs, thus reducing the number of electrons that can screen the piezoelectric potential, as shown in Fig. 1**e (ii)**. The p-n junction device is therefore able to suppress the screening effect and thus enhance the piezoelectric output.

An enlarged schematic of the ZnO-Si p-n junction is shown in Fig. 2**a.** Such a layered structure was successfully verified by surface and cross-sectional SEM images, as shown in Fig. 2**b**. As can be seen, the ZnO NRs have a strict orientation along the c-axis with an average height of 2 μm and an average diameter of 120 nm (See the statistical average diameter plot in **Figure S1**), which is

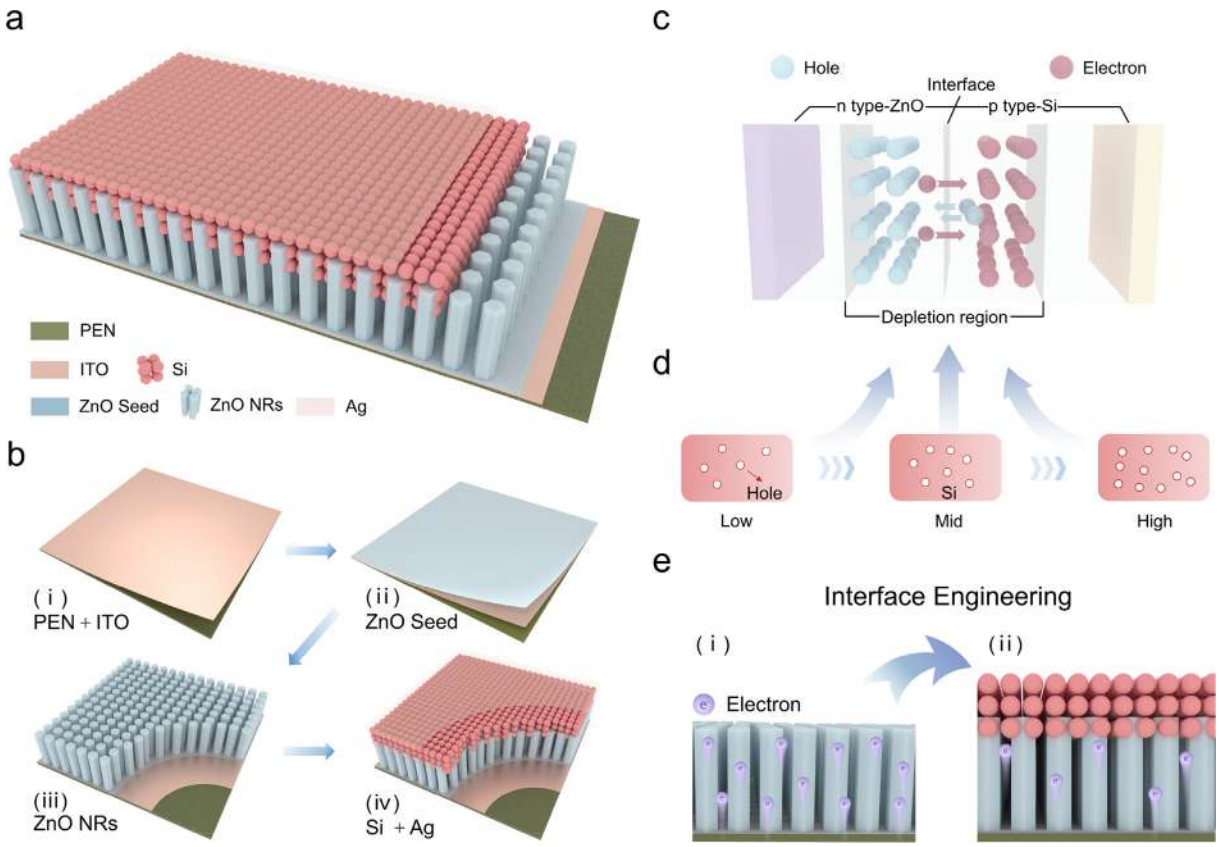

Fig. 1. The schematic diagrams of the device structure and interface engineering. The schematic diagram (a) and the detailed preparation (b) of ZnO-based p-n junction piezoelectric device. (c) Schematic diagram of electrons and holes motion and distribution at the interface of ZnO-Si. (d) Si films with different carrier concentrations as p-type semiconductor for interface engineering. (e) Schematic illustration of the electrons for screening effect in intrinsic ZnO NRs (i) and interface engineered ZnO NRs (ii).

beneficial for the preparation of piezoelectric devices. In addition, low-magnification surface and cross-sectional SEM images of the ZnO NRs (Figure S1) and corresponding EDS mapping (**Figure S2**) further confirm that the ZnO films exhibit good homogeneity. As seen from the high-magnification SEM images of the ZnO-Si (D-4) p-n junction device (Fig. 2**c**), the p-type Si films are uniformly deposited on the surface of the ZnO NRs and wrapped around the top of the nanorods. This structure is further demonstrated by the corresponding cross-sectional (Fig. 2**d**) and surface (**Figure S3**) EDS mapping as well as the other four devices (**Figure S4**). From the results, it can be observed that the carrier concentration does not affect the morphology of the films, which facilitates the subsequent preparation and characterization analysis. The X-ray diffraction patterns (**Figure S5**) reveal the crystal structure of the grown ZnO NRs and Si films. The remarkably intense diffraction peak at 34.58° originates from the (002) plane of the ZnO NRs, indicating that they preferentially grow along the c-axis perpendicular to the ITO substrate, which is also verified by the cross-sectional SEM images of the ZnO NRs [23]. In contrast, the Si films show broad peaks, which indicates that the Si films obtained by magnetron sputtering are amorphous. Also in the Raman spectrum (Fig. 2**e**), there is no significant scattering peak, and only a scattering packet at 480 cm^{-1}, which is perfectly consistent with the XRD results of the amorphous Si films [33]. All these characterizations demonstrate the successful preparation of ZnO NRs and Si films, as well as the ZnO-Si p-n junction.

The accurate measurement of carrier concentration is essential to evaluate the depletion region and the built-in electric field of the p-n junction. To measure the surface carrier concentration of p-type Si films and ZnO NRs, Mott-Schottky plots of the semiconductor electrolyte interface were obtained from AC impedance measurements (Fig. 2**f**-**h**). The Mott-Schottky equation allows the carrier concentration to be calculated [34,35]:

$$\left(\frac{1}{C}\right)^2 = \left(\frac{2}{A^2 e \varepsilon_s \varepsilon_0 N}\right)\left[(V_R - V_{FB}) - \frac{kT}{e}\right] \quad (1)$$

Where C denotes the capacitance of the space charge region, V_R is the externally applied bias voltage, A is the tested area, ε_s is the dielectric constant, ε_0 is the vacuum dielectric constant, V_{FB} is the flat band potential, k is the Boltzmann constant, T is the temperature, e is the meta-charge and N is the carrier concentration. The slope of the curve was obtained by fitting the linear region of the curve of $1/C^2$-V. From the results, the slopes of the fitted straight lines are negative and positive in Si films and ZnO NRs, indicating that the prepared Si films and ZnO NRs are p-type and n-type semiconductors, respectively. And the carrier concentrations of the prepared ZnO NRs and Si (S-1, S-2, S-3, S-4, S-5) films are calculated to be 1.6×10^{16} cm^{-3}, 2.04×10^{17} cm^{-3}, 4.77×10^{17} cm^{-3}, 1.32×10^{18} cm^{-3}, 7.88×10^{18} cm^{-3}, 1.44×10^{19} cm^{-3}, as shown in Fig. 2**i**. Furthermore, the built-in electric field (V_{bi}) of the ZnO-Si p-n junction can be estimated by the following equation [27].

$$V_{bi} = \frac{k_B T}{e} ln\left(\frac{N_d N_a}{n_i^p n_i^n}\right) \quad (2)$$

Where n_i is the intrinsic carrier concentration of the material, N_a and N_d are the carrier concentrations of the p-type and n-type layers, respectively. From the equation, the built-in electric field increases with the carrier concentration in the p-type layer when the ZnO NRs are kept constant. The built-in electric fields of the

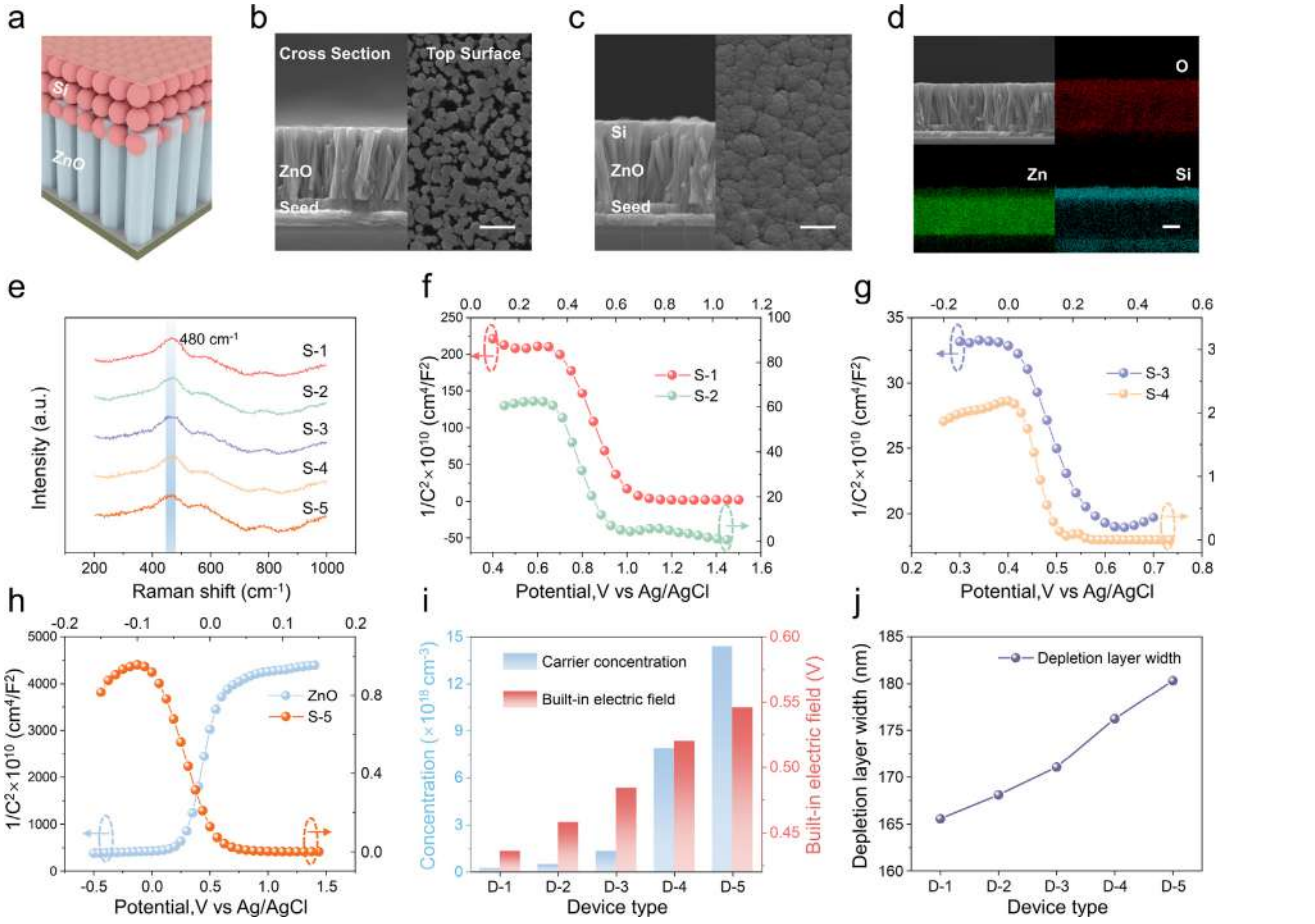

Fig. 2. The microscopic morphology and structural characterization. (a) Schematic cross-section of a ZnO-Si p-n junction device. Cross-sectional and surface morphology SEM images of ZnO NRs (b) and ZnO-Si (D-4) (c). (d) Corresponding cross-sectional EDS mapping of ZnO-Si (D-4) p-n junction device. (e) Raman spectra of Si (S-1, S-2, S-3, S-4, S-5) films on glass substrate. (f-g) Mott-Schottky plots of the ZnO NRs and Si (S-1, S-2, S-3, S-4, S-5) films on ITO substrate from electrochemical analysis in an aqueous system. (i) Carrier concentration and built-in electric field of ZnO-Si (D-1, D-2, D-3, D-4, D-5) p-n junction devices. (j) Depletion region width of ZnO-Si (D-1, D-2, D-3, D-4, D-5) p-n junction devices. All the scale bars are 1 μm.

ZnO-Si p-n junctions (D-1, D-2, D-3, D-4, D-5) are calculated to be 0.4359 V, 0.4578 V, 0.4840 V, 0.5202 V and 0.5458 V, respectively (Fig. 2i). On this basis, the depletion region width (W) of the ZnO-Si p-n junction can therefore be calculated according to the following equation:

$$W = \left\{ \frac{2\varepsilon_s V_{bi}}{e} \left[\frac{N_a + N_d}{N_a N_d} \right] \right\}^{1/2} \quad (3)$$

The depletion region widths of ZnO-Si (D-1, D-2, D-3, D-4, D-5) p-n junctions were calculated to be 165.57 nm, 168.11 nm, 171.06 nm, 176.24 nm, 180.32 nm, respectively (Fig. 2**j**). Apparently, both the depletion region width and the built-in electric field of the ZnO-Si p-n junction increase with the carrier concentration of the p-type Si films. The successful construction of ZnO-Si p-n junction devices with different carrier concentrations has laid the foundation for subsequent electrical performance studies.

From the *I-V* curves, the ZnO-Si p-n junction devices (Fig. 3**a**) exhibit excellent rectification characteristics compared to that of ZnO NRs (**Figure S6**), which also demonstrates the successful preparation of ZnO-Si p-n junction devices. In addition, the currents of the devices (D-1 to D-5) gradually increase at the same forward bias, indicating a gradual increase of carrier concentration in the Si film (S-1 to S-5), which corroborates the results of previous carrier concentration tests. Furthermore, the piezoelectric output voltages and currents (Fig. 3**b**) of the devices were measured 3 times for each device with a periodic pressure of 2 MPa. The detailed output voltages and currents are shown in **Figures S7 and S8,** respectively. A set of samples are selected to investigate the relationship between p-type carrier concentration and piezoelectric output (Fig. 3**c**). From the results, it can be seen that the piezoelectric outputs increase significantly after forming the p-n junction through interface engineering. Specifically, the average output voltage and current of ZnO-Si (D-4) reach 0.89 V and 44.6 nA, respectively, which is about 12 times higher than that of ZnO-pure device. The polarity switching test shown in Fig. 3**d** demonstrates that the polarity of the output signal flips with the switching of the electrode connection, confirming that the output performance originated from piezoelectric effect rather than the friction of the test. The detailed output voltages (**Figure S9**) and currents (**Figure S10**) of all devices were also measured under other different pressures, and their variations are shown in Fig. 3**e**. As can be seen that the output of all devices increased with pressure, and the device D-4 showed the best performance over the entire pressure range. Furthermore, the sensitivities of the devices were calculated by fitting the piezoelectric output voltage at different pressures (Fig. 3**f**). Obviously, the sensitivity shows a trend of increasing and then slightly decreasing from D-1 to D-5, with the highest sensitivity of D-4 reaching 384.7 mV MPa^{-1}. In addition, the piezoelectric output voltage remained essentially constant after 2700 cycles with a loading pressure of 1.5 MPa at 1.5 Hz, clearly revealing the high mechanical stability and

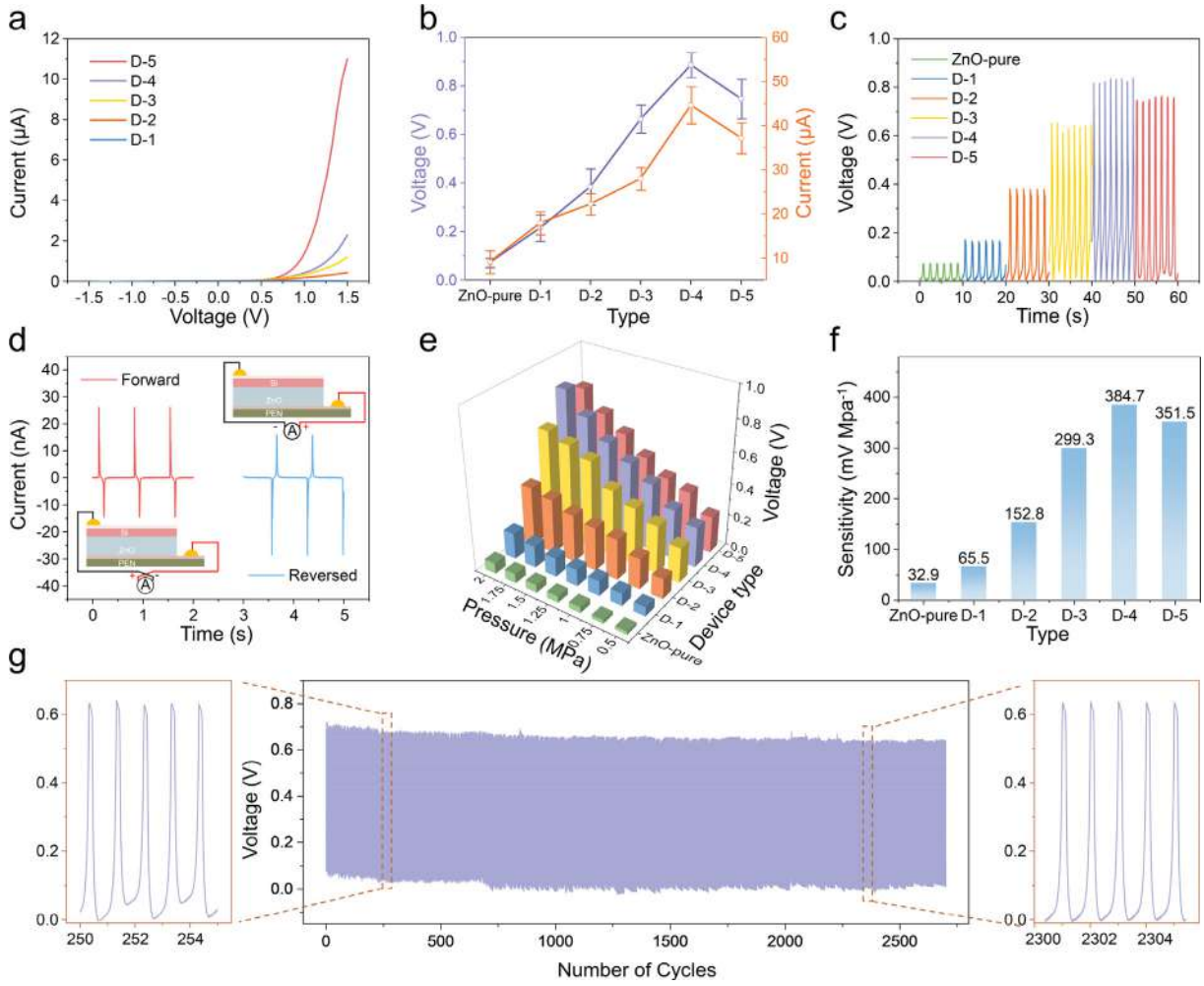

Fig. 3. Electrical performance measurement of devices. (a) The *I-V* curves of ZnO-Si (D-1, D-2, D-3, D-4, D-5) p-n junction devices. (b) The output voltages and currents of ZnO-Si p-n junction devices under the pressure of 2 MPa. (c) Relationship between p-type carrier concentration and piezoelectric output voltages. (d) Schematic illustration of forward and backward connection and the corresponding piezoelectric outputs. (e) The effect of pressure on the output voltage of ZnO-pure and ZnO-Si p-n junction devices. (f) The sensitivity of ZnO-pure and ZnO-Si p-n junction devices. (g) Durability test results of ZnO-Si (D-4) p-n junction device.

durability of ZnO-Si p-n junction device prepared by interface engineering (Fig. 3**g**). In summary, the piezoelectric output of ZnO NRs is significantly enhanced by the construction of ZnO-Si p-n junctions, and exhibits excellent stability.

To further investigate the enhancement mechanism of ZnO-Si p-n junction devices, a series of theoretical simulations and experimental tests were conducted. Fig. 4**a** schematically depicts the carrier distribution and energy band structure at the interface of the ZnO-Si p-n junction with different carrier concentrations. Among them, the depletion region width and the built-in electric field of the p-n junction increase with the carrier concentration, as demonstrated in Fig. 2i and 2j. From the carrier concentration distribution in the depletion region of p-n junction (**Figure S11**), the number of carriers confined in the depletion region can be calculated by integrating the carrier concentration over the width of the depletion region. This means that a higher p-type semiconductor carrier concentration and a wider depletion region can confine more carriers, which further reduces the number of free electrons in the ZnO NRs that can screen the piezoelectric potential and thus increase the piezoelectric output. In addition, the larger built-in electric field in the p-n junction attenuates the depolarizing electric field that drives the screening charges on the surface of the ZnO NRs, thus suppressing the screening effect more effectively. Therefore, as the carrier concentration of the p-type Si film increases, the suppression of the screening effect becomes more pronounced and the piezoelectric output shows a significant enhancement as displayed in Fig. 4**b**. However, the piezoelectric potential of the device does not always increase with decreasing the free electrons in ZnO NRs. From the simulation results of the piezoelectric potential versus carrier concentration in ZnO NRs (Fig. 4**c**), it can be observed that the piezoelectric potential first increases significantly and then tend to be stable with decreasing the carrier concentration of ZnO NRs. This indicates that the screening effect on the piezoelectric potential of ZnO NRs is negligible when the carrier concentration is below a certain level (The screening effect can be considered invalid). On the other hand, when the carrier concentration of p-type semiconductor keeps increasing, the total capacitance of the p-n junction device also increases, which is detrimental to the piezoelectric output. The total capacitance of the p-n junction device includes the capacitance of the ZnO NRs and the ZnO-Si p-n junction connected in series, and is less than either one of them. According to $Q = CV$, where Q is the charge, C is the capacitance, and V is the voltage, a lower device capacitance can boost the piezoelectric potential under the same piezoelectric charge density. To further test the variation in total device capacitance, the electrochemical impedance spectra of ZnO NRs and ZnO-Si p-n junctions were measured as shown in Fig. 4**d and 4e**. The two typical semicircular arc plots with negative

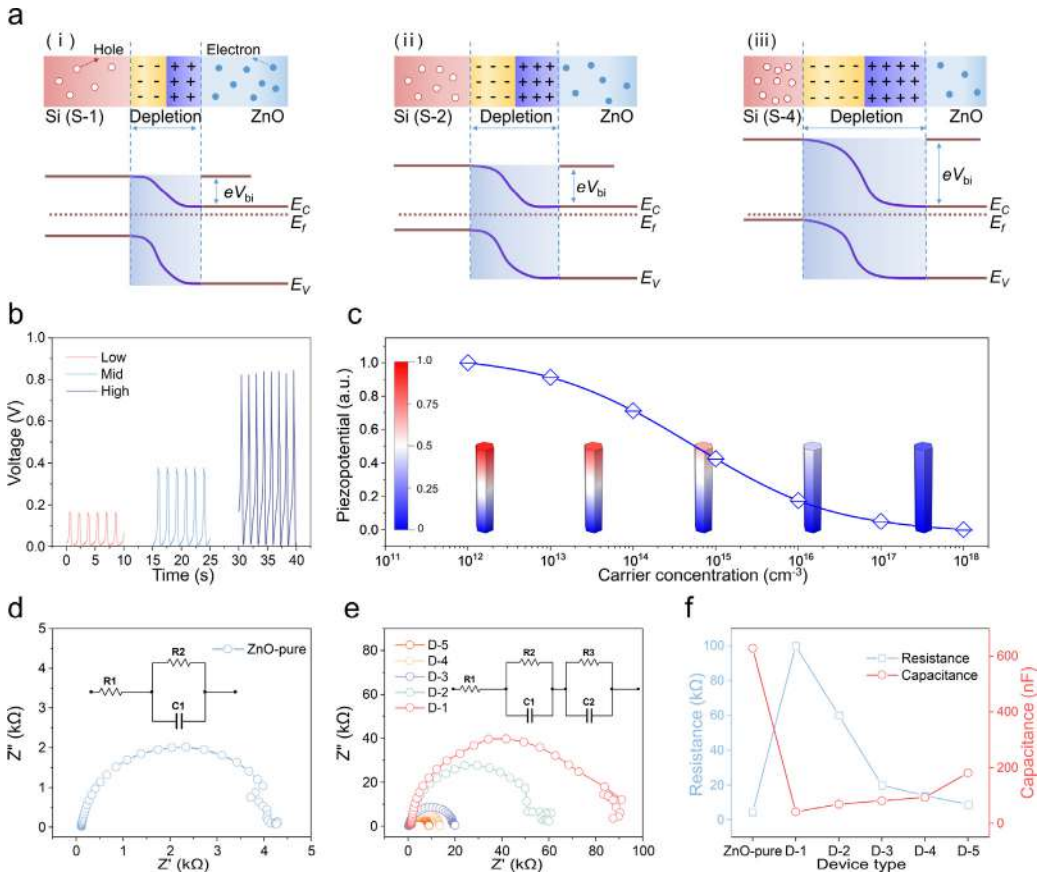

Fig. 4. Study of the enhancement mechanism. (a) Variation of carrier distribution and energy band at ZnO-Si p-n junction interface with increasing hole concentration in p-type Si films, and the corresponding change in piezoelectric output voltage (b). (c) The calculated piezopotential of ZnO NRs under different electron concentrations. Electrochemical impedance spectra of ZnO-pure (d) and ZnO-Si (D-1, D-2, D-3, D-4, D-5) p-n junction (e) devices, and corresponding resistance and capacitance (f), respectively.

fictitious impedance imply the presence of an *RC* circuit where the equivalent resistance *R* is close to the diameter of the arc [36,37]. Combined with the characteristic frequency f_c, the device capacitance *C* can be calculated ($\tau = RC = 1/2\pi f_c$) as shown in Fig. 4**f**. With the increasing of the carrier concentration of p-type Si film, the equivalent resistance decreases and the total capacitance increases, which is undoubtedly detrimental to the piezoelectric output. As the carrier concentration of p-type Si film continues to increase, the reduction of the device capacitance on the piezoelectric output outweighs the enhancement of suppressing screening effect on the piezoelectric output, resulting in a decrease in the final output of the device. Thus, the piezoelectric output tends to increase and then decrease from D-1 to D-5, and reaches the maximum at D-4. Undoubtedly, the carrier concentration of p-type semiconductor is particularly important for p-n junction piezoelectric devices based on ZnO NRs. There is a matched design for the carrier concentration, which balances the trade-off between the screening effect and the device capacitance to obtain the optimal electrical output of piezoelectric semiconductor devices.

4. Conclusion

In summary, the enhancement mechanism of carrier concentration-dependent interface engineering on piezoelectric performance has been systematically investigated in ZnO NRs-based p-n junction piezoelectric devices. The p-type Si films with different carrier concentrations were fabricated on the surface of ZnO NRs to form p-n junctions, which significantly improved the piezoelectric performance (about 12 times) by suppressing the screening effect. More importantly, the piezoelectric output of p-n junction devices shows a trend of increasing and then slightly decreasing with increasing p-type semiconductor carrier concentration. When designing ZnO NRs-based p-n junction devices, the screening effect and the device capacitance on the piezoelectric output need to be considered simultaneously, and a matched p-type semiconductor carrier concentration will be available to achieve the optimal piezoelectric performance of the device. Notably, this work provides further insight into the mechanism of interface engineering on the regulation of ZnO NRs-based piezoelectric devices and offers a reasonable idea for the design of efficient p-n junction piezoelectric devices.

CRediT authorship contribution statement

Hongrui Zhang: Writing - review & editing. **Guo Tian:** Data curation. **Da Xiong:** Formal analysis. **Tao Yang:** Investigation. **Shenglong Wang:** Methodology. **Yue Sun:** Resources. **Long Jin:** Formal analysis. **Boling Lan:** Validation. **Lin Deng:** Visualization. **Weiqing Yang:** Funding acquisition. **Weili Deng:** Conceptualization & supervision.

Declaration of Competing Interest

The authors declare that they have no known competing financial interests or personal relationships that could have appeared to influence the work reported in this paper.

Acknowledgements

This research was financially supported by the National Natural Science Foundation of China (No.61801403), the Sichuan Province Foundation for Distinguished Young Team (No.20CXTD0106), the Basic Research Cultivation Project (No.2682021ZTPY004). Thanks for the help from the Analysis and Testing Center of Southwest Jiaotong University.

Appendix A. Supplementary data

Supplementary data to this article can be found online at https://doi.org/10.1016/j.jcis.2022.08.181.

References

[1] Y. Dobashi, D. Yao, Y. Petel, T.N. Nguyen, M.S. Sarwar, Y. Thabet, C.L.W. Ng, E. Scabeni Glitz, G.T.M. Nguyen, C. Plesse, F. Vidal, C.A. Michal, J.D.W. Madden, Piezoionic mechanoreceptors: Force-induced current generation in hydrogels, Science 376 (6592) (2022) 502–507.
[2] S. Zhong, D.a. Xiong, B. Zhang, X. Yang, T. Yang, G. Tian, H. Zhang, W. Yang, W. Deng, Structurally unraveling the photocarrier behavior of Cu_2O/ZnO heterojunction photodetectors, ACS Photonics 9 (1) (2022) 268–274.
[3] T. Yang, W. Deng, X. Chu, X. Wang, Y. Hu, X.i. Fan, J. Song, Y. Gao, B. Zhang, G. Tian, D.a. Xiong, S. Zhong, L. Tang, Y. Hu, W. Yang, Hierarchically microstructure-bioinspired flexible piezoresistive bioelectronics, ACS Nano 15 (7) (2021) 11555–11563.
[4] W. Deng, Y. Zhou, A. Libanori, G. Chen, W. Yang, J. Chen, Piezoelectric nanogenerators for personalized healthcare, Chem. Soc. Rev. 51 (9) (2022) 3380–3435.
[5] T. Yang, H. Pan, G. Tian, B. Zhang, D.a. Xiong, Y. Gao, C. Yan, X. Chu, N. Chen, S. Zhong, L. Zhang, W. Deng, W. Yang, Hierarchically structured PVDF/ZnO core-shell nanofibers for self-powered physiological monitoring electronics, Nano Energy 72 (2020) 104706.
[6] W. Yan, G. Noel, G. Loke, E. Meiklejohn, T. Khudiyev, J. Marion, G. Rui, J. Lin, J. Cherston, A. Sahasrabudhe, J. Wilbert, I. Wicaksono, R.W. Hoyt, A. Missakian, L. Zhu, C. Ma, J. Joannopoulos, Y. Fink, Single fibre enables acoustic fabrics via nanometre-scale vibrations, Nature 603 (7902) (2022) 616–623.
[7] G. Tian, W. Deng, D.a. Xiong, T. Yang, B. Zhang, X. Ren, B. Lan, S. Zhong, L. Jin, H. Zhang, L. Deng, W. Yang, Dielectric micro-capacitance for enhancing piezoelectricity via aligning MXene sheets in composites, Cell Rep. Phys. Sci. 3 (4) (2022) 100814.
[8] G. Tian, W. Deng, Y. Gao, D. Xiong, C. Yan, X. He, T. Yang, L. Jin, X. Chu, H. Zhang, W. Yan, W. Yang, Rich lamellar crystal baklava-structured PZT/PVDF piezoelectric sensor toward individual table tennis training, Nano Energy 59 (2019) 574–581.
[9] W. Deng, T. Yang, L. Jin, C. Yan, H. Huang, X. Chu, Z. Wang, D. Xiong, G. Tian, Y. Gao, H. Zhang, W. Yang, Cowpea-structured PVDF/ZnO nanofibers based flexible self-powered piezoelectric bending motion sensor towards remote control of gestures, Nano Energy 55 (2019) 516–525.
[10] Q. Zheng, M. Peng, Z. Liu, S. Li, R. Han, H. Ouyang, Y. Fan, C. Pan, W. Hu, J. Zhai, Z. Li, Z.L. Wang, Dynamic real-time imaging of living cell traction force by piezo-phototronic light nano-antenna array, Sci. Adv. 7 (2021) eabe7738.
[11] Q. Yu, R. Ge, J. Wen, T. Du, J. Zhai, S. Liu, L. Wang, Y. Qin, Highly sensitive strain sensors based on piezotronic tunneling junction, Nat. Commun. 13 (2022) 778.
[12] W. Wu, X. Wen, Z.L. Wang, Taxel-addressable matrix of vertical-nanowire piezotronic transistors for active and adaptive tactile imaging, Science 340 (6135) (2013) 952–957.
[13] L. Wang, S. Liu, G. Gao, Y. Pang, X. Yin, X. Feng, L. Zhu, Y.u. Bai, L. Chen, T. Xiao, X. Wang, Y. Qin, Z.L. Wang, Ultrathin piezotronic transistors with 2 nm channel lengths, ACS Nano 12 (5) (2018) 4903–4908.
[14] L. Wang, S. Liu, Z. Zhang, X. Feng, L. Zhu, H. Guo, W. Ding, L. Chen, Y. Qin, Z.L. Wang, 2D piezotronics in atomically thin zinc oxide sheets: Interfacing gating and channel width gating, Nano Energy 60 (2019) 724–733.
[15] S. Liu, L. Wang, Z. Wang, Y. Cai, X. Feng, Y. Qin, Z.L. Wang, Double-channel piezotronic transistors for highly sensitive pressure sensing, ACS Nano 12 (2) (2018) 1732–1738.
[16] S. Liu, L. Wang, X. Feng, Z. Wang, Q.i. Xu, S. Bai, Y. Qin, Z.L. Wang, Ultrasensitive 2D ZnO piezotronic transistor array for high resolution tactile imaging, Adv. Mater. 29 (16) (2017) 1606346.
[17] C. An, H. Qi, L. Wang, X. Fu, A. Wang, Z.L. Wang, J. Liu, Piezotronic and piezo-phototronic effects of atomically-thin ZnO nanosheets, Nano Energy 82 (2021) 105653.
[18] X. Li, M. Chen, R. Yu, T. Zhang, D. Song, R. Liang, Q. Zhang, S. Cheng, L. Dong, A. Pan, Z.L. Wang, J. Zhu, C. Pan, Enhancing light emission of ZnO-nanofilm/Si-micropillar heterostructure arrays by piezo-phototronic effect, Adv. Mater. 27 (30) (2015) 4447–4453.
[19] R. Bao, C. Wang, L. Dong, R. Yu, K. Zhao, Z.L. Wang, C. Pan, Flexible and controllable piezo-phototronic pressure mapping sensor matrix by ZnO NW/p-Polymer LED array, Adv. Funct. Mater. 25 (19) (2015) 2884–2891.
[20] M. Chen, C. Pan, T. Zhang, X. Li, R. Liang, Z.L. Wang, Tuning light emission of a pressure-sensitive silicon/ZnO nanowires heterostructure matrix through piezo-phototronic effects, ACS Nano 10 (6) (2016) 6074–6079.
[21] G. Tian, D.a. Xiong, Y. Su, T. Yang, Y. Gao, C. Yan, W. Deng, L. Jin, H. Zhang, X. Fan, C. Wang, W. Deng, W. Yang, Understanding the potential screening effect through the discretely structured ZnO nanorods piezo array, Nano Lett. 20 (6) (2020) 4270–4277.
[22] J.I. Sohn, S.N. Cha, B.G. Song, S. Lee, S.M. Kim, JiYeon Ku, H.J. Kim, Y.J. Park, B.L. Choi, Z.L. Wang, J.M. Kim, K. Kim, Engineering of efficiency limiting free carriers and an interfacial energy barrier for an enhancing piezoelectric generation, Energy Environ. Sci. 6 (1) (2013) 97–104.
[23] Z. Huo, X. Wang, Y. Zhang, B. Wan, W. Wu, J. Xi, Z. Yang, G. Hu, X. Li, C. Pan, High-performance Sb-doped p-ZnO NW films for self-powered piezoelectric strain sensors, Nano Energy 73 (2020) 104744.
[24] Y.-L. Su, K. Gupta, Y.-L. Hsiao, R.-C. Wang, C.-P. Liu, Gigantic enhancement of electricity generation in piezoelectric semiconductors by creating pores as a universal approach, Energy Environ. Sci. 12 (1) (2019) 410–417.
[25] K.Y. Lee, B. Kumar, J.-S. Seo, K.-H. Kim, J.I. Sohn, S.N. Cha, D. Choi, Z.L. Wang, S.-W. Kim, p-Type polymer-hybridized high-performance piezoelectric nanogenerators, Nano Lett. 12 (4) (2012) 1959–1964.
[26] J. Briscoe, M. Stewart, M. Vopson, M. Cain, P.M. Weaver, S. Dunn, Nanostructured p-n junctions for kinetic-to-electrical energy conversion, Adv. Energy Mater. 2 (10) (2012) 1261–1268.
[27] H. Zhang, G. Tian, D.a. Xiong, T. Yang, S. Zhong, L. Jin, B. Lan, L. Deng, S. Wang, Y. Sun, W. Yang, W. Deng, Understanding the enhancement mechanism of ZnO nanorod-based piezoelectric devices through surface engineering, ACS Appl. Mater. Interfaces 14 (25) (2022) 29061–29069.
[28] Q. He, X. Li, J. Zhang, H. Zhang, J. Briscoe, P-N junction-based ZnO wearable textile nanogenerator for biomechanical energy harvesting, Nano Energy 85 (2021) 105938.
[29] B. Yin, Y. Qiu, H. Zhang, J. Lei, Y. Chang, J. Ji, Y. Luo, Y. Zhao, L. Hu, Piezoelectric performance enhancement of ZnO flexible nanogenerator by a NiO–ZnO p–n junction formation, Nano Energy 14 (2015) 95–101.
[30] K.Y. Lee, J. Bae, S. Kim, J.-H. Lee, G.C. Yoon, M.K. Gupta, S. Kim, H. Kim, J. Park, S.-W. Kim, Depletion width engineering via surface modification for high performance semiconducting piezoelectric nanogenerators, Nano Energy 8 (2014) 165–173.
[31] C. Liu, M. Peng, A. Yu, J. Liu, M. Song, Y. Zhang, J. Zhai, Interface engineering on p-CuI/n-ZnO heterojunction for enhancing piezoelectric and piezo-phototronic performance, Nano Energy 26 (2016) 417–424.
[32] D.a. Xiong, W. Deng, G. Tian, Y. Gao, X. Chu, C. Yan, L. Jin, Y. Su, W. Yan, W. Yang, A piezo-phototronic enhanced serrate-structured ZnO-based heterojunction photodetector for optical communication, Nanoscale 11 (6) (2019) 3021–3027.
[33] T. Wang, H. Yan, M. Zhang, X. Song, Q. Pan, T. He, Z. Hu, H. Jia, Y. Mai, Polycrystalline silicon thin films by aluminum induced crystallization of amorphous silicon, Appl. Surf. Sci. 264 (2013) 11–16.
[34] P. Lin, X. Chen, X. Yan, Z. Zhang, H. Yuan, P. Li, Y. Zhao, Y. Zhang, Enhanced photoresponse of Cu_2O/ZnO heterojunction with piezo-modulated interface engineering, Nano Res. 7 (6) (2014) 860–868.
[35] T. E, Z. Ma, D. Cai, S. Yang, Y. Li, Enhancement of interfacial charge transfer of TiO_2/Graphene with doped Ca^{2+} for improving electrical conductivity, ACS Appl. Mater. Interfaces 13 (35) (2021) 41875–41885.
[36] S. Lu, Q. Liao, J. Qi, S. Liu, Y. Liu, Q. Liang, G. Zhang, Y. Zhang, The enhanced performance of piezoelectric nanogenerator via suppressing screening effect with Au particles/ZnO nanoarrays schottky junction, Nano Res. 9 (2) (2016) 372–379.
[37] P. Ghamgosar, F. Rigoni, S. You, I. Dobryden, M.G. Kohan, A.L. Pellegrino, I. Concina, N. Almqvist, G. Malandrino, A. Vomiero, ZnO-Cu_2O core-shell nanowires as stable and fast response photodetectors, Nano Energy 51 (2018) 308–316.